

Acknowledgements

This work was partially supported by The Petroleum Research Fund.

Correspondence and requests for materials should be addressed to H.A.M. (e-mail: makse@mailaps.org).

Growth of nanowire superlattice structures for nanoscale photonics and electronics

Mark S. Gudiksen^{*†}, Lincoln J. Lauhon^{*†}, Jianfang Wang^{*}, David C. Smith^{*‡} & Charles M. Lieber^{*§}

^{*} Department of Chemistry and Chemical Biology, [§] Division of Engineering and Applied Sciences, Harvard University, Cambridge, Massachusetts 02138, USA

[†] These authors contributed equally to this work

The assembly of semiconductor nanowires and carbon nanotubes into nanoscale devices and circuits could enable diverse applications in nanoelectronics and photonics¹. Individual semiconducting nanowires have already been configured as field-effect transistors², photodetectors³ and bio/chemical sensors⁴. More sophisticated light-emitting diodes⁵ (LEDs) and complementary and diode logic^{6–8} devices have been realized using both n- and p-type semiconducting nanowires or nanotubes. The n- and p-type materials have been incorporated in these latter devices either by crossing p- and n-type nanowires^{2,5,6,9} or by lithographically defining distinct p- and n-type regions in nanotubes^{8,10}, although both strategies limit device complexity. In the planar semiconductor industry, intricate n- and p-type and more generally compositionally modulated (that is, superlattice) structures are used to enable versatile electronic and photonic functions. Here we demonstrate the synthesis of semiconductor nanowire superlattices from group III–V and group IV materials. (The superlattices are created within the nanowires by repeated modulation of the vapour-phase semiconductor reactants during growth of the wires.) Compositionally modulated superlattices consisting of 2 to 21 layers of GaAs and GaP have been prepared. Furthermore, n-Si/p-Si and n-InP/p-InP modulation doped nanowires have been synthesized. Single-nanowire photoluminescence, electrical transport and electroluminescence measurements show the unique photonic and electronic properties of these nanowire superlattices, and suggest potential applications ranging from nano-barcodes to polarized nanoscale LEDs.

Our approach to superlattice growth (Fig. 1) exploits recent developments in metal-catalysed nanowire synthesis, which have shown that nearly monodisperse metal nanoclusters can be used to control the diameter^{11,12} and (through growth time) the length¹³ of group III–V and group IV semiconductor nanowires by way of a vapour–liquid–solid growth process¹⁴. We introduce the vapour-phase semiconductor reactants required for nanowire growth by either laser ablation of solid targets^{15,16} or vapour-phase molecular species^{12,17}. To create a single junction within the nanowire, the addition of the first reactant is stopped during growth, and then a second reactant is introduced for the remainder of the synthesis (Fig. 1b); repeated modulation of the reactants during growth produces nanowire superlattices (Fig. 1c). In principle, this

approach can be successfully implemented if a nanocluster catalyst suitable for growth of the different superlattice components under similar conditions is found; our previous studies¹⁶ suggest that Au nanoclusters meet this requirement for a wide range of III–V and IV materials.

Gallium arsenide (GaAs)/gallium phosphide (GaP) superlattices have been grown by laser-assisted catalytic growth using GaAs and GaP targets. Figure 2 shows transmission electron microscopy (TEM) images of the products of this synthesis. It is relatively straightforward to focus on the junction area as the nanowire lengths can be controlled directly by growth times¹³. High-resolution TEM images of a typical GaAs/GaP junction region (Fig. 2a) exhibit a crystalline nanowire core without obvious defects, and show that the nanowire axes lies along the $\langle 111 \rangle$ direction, in agreement with previous studies of single-component systems^{11,13,15,16}. Two-dimensional Fourier transforms calculated from high-resolution images containing the junction region (Fig. 2a, inset) show pairs of reciprocal lattice peaks along the different lattice directions, while such transforms calculated from the regions above and below the junction (not shown) exhibit only single reciprocal lattice peaks. Analysis of these peak data yield lattice constants, indexed to the zinc blende structures of GaP and GaAs, of 0.5474 ± 0.0073 nm and 0.5668 ± 0.0085 nm, and are in good agreement with the values for both GaP (0.5451 nm) and GaAs (0.5653 nm), respectively.

The TEM structural data suggest that the GaP/GaAs junctions could be abrupt, and thus we have carried out local elemental mapping of the heterojunction by energy dispersive X-ray spectroscopy (EDS) to address composition variation across the junction (Fig. 2b–e). These elemental maps show that Ga is uniformly distributed along the length of the nanowire, while P (Fig. 2d) and As (Fig. 2e) appear localized in the GaP and GaAs portions of the nanowire heterostructure, respectively. Quantitative analysis of the P and As composition variation (Fig. 2f) shows, however, that the junction is not atomically abrupt, but rather makes the transition between GaP and GaAs phases over a length scale of 15–20 nm. This length scale is reasonable considering that the ~20-nm-diameter Au catalyst must re-alloy with GaP after initial GaAs growth. The observed composition variation has several potentially important implications. First, composition variation at the interface can relieve strain, and may enable the defect-free junctions and superlattices that we observe in this system—which has a relatively large lattice mismatch. We note, however, that simple estimates of the length between dislocations (M.S.G. and C.M.L., unpublished results) suggest that defect-free, atomically abrupt interfaces may be possible in wires of diameter less than 20 nm. Second, there are photonic and electronic applications where abrupt interfaces are important. The observed composition variation could be substantially reduced in smaller-diameter nanowires; that is, a 5-nm-

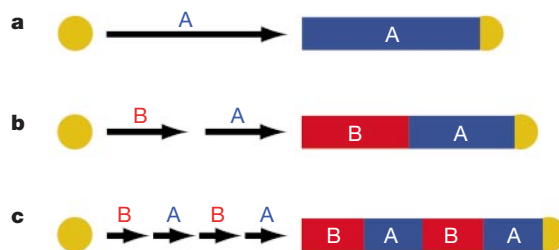


Figure 1 Synthesis of nanowire superlattices. **a**, A nanocluster catalyst (shown gold) nucleates and directs one-dimensional semiconductor nanowire (blue) growth with the catalyst remaining at the terminus of the nanowire. **b**, Upon completion of the first growth step, a different material (red) can be grown from the end of the nanowire. **c**, Repetition of steps **a** and **b** leads to a compositional superlattice within a single nanowire.

[‡]Present address: Department of Physics and Astronomy, University of Southampton, Highfield, Southampton SO17 1BJ, UK.

diameter nanowire superlattice should have variations of <5 nm across the junction interfaces. Alternatively, it should be possible to use different nanocluster catalysts or variations in the growth temperature when reactants are switched to obtain sharper interfaces.

We find that this approach can produce compositionally modulated nanowire superlattices in which the number of periods and repeat spacing can be readily varied during growth. TEM images of a six-period structure corresponding to a $(\text{GaP}/\text{GaAs})_3$ superlattice (Fig. 3a) show that the 20-nm-diameter nanowires are highly uniform over their $\sim 3\text{-}\mu\text{m}$ lengths. Spatially resolved EDS measurements of composition (Fig. 3b) further demonstrate that the P and As regions are distinct from one another, and that there is minimal cross-contamination. Moreover, these data show that each GaP and GaAs nanowire segment has a length of about 500 nm, and are thus consistent with the equal growth times used for each segment, but also show that growth rates remain relatively constant during the entire nanowire synthesis.

GaAs/GaP nanowire superlattices are an attractive system to explore for nano-phonic applications because GaAs is a direct bandgap semiconductor, while GaP has an indirect gap. Indeed, photoluminescence imaging of individual nanowires from the $(\text{GaP}/\text{GaAs})_3$ superlattice sample described above shows that these nanowires exhibit an emission pattern of three spots separated by dark regions (Fig. 3c). This pattern is consistent with emission

originating from the three GaAs regions, separated by dark GaP regions that act as optical 'spacers'. Control experiments on individual samples of pure GaAs and GaP nanowires confirm that strong luminescence is obtained from GaAs but not GaP, as expected. The GaAs regions also exhibit a strong polarization dependence, emitting when the excitation is polarized parallel (\parallel) to the nanowire axis and appearing dark when the polarization is perpendicular (\perp) to the nanowire axis (Fig. 3c, inset). In addition, experiments (M.S.G., D.C.S. and C.M.L., unpublished results) show that the emission from the superlattice structures is also highly polarized along the wire axis. These results are consistent with recently reported photoluminescence spectroscopy of single InP nanowires³, and could enable several unique applications (see below).

We have also used single-nanowire photoluminescence studies to assess the level of control possible in nanowire superlattice growth by our approach. Specifically, we find that systematic variations in the growth time produces nanowire superlattices with well-defined changes in periodicity. The photoluminescence image of an 11-layer superlattice in which the length of the GaP regions was doubled each layer while maintaining a constant GaAs period (Fig. 3d) shows clearly that the separation between emitting GaAs regions is doubling along the length of the nanowire. In addition, the power and promise of this approach can be seen clearly in photoluminescence spectra of 21-layer GaP/GaAs superlattices (Fig. 3e) consisting of a short 4-period (GaP/GaAs) repeat, followed by 3 longer GaP

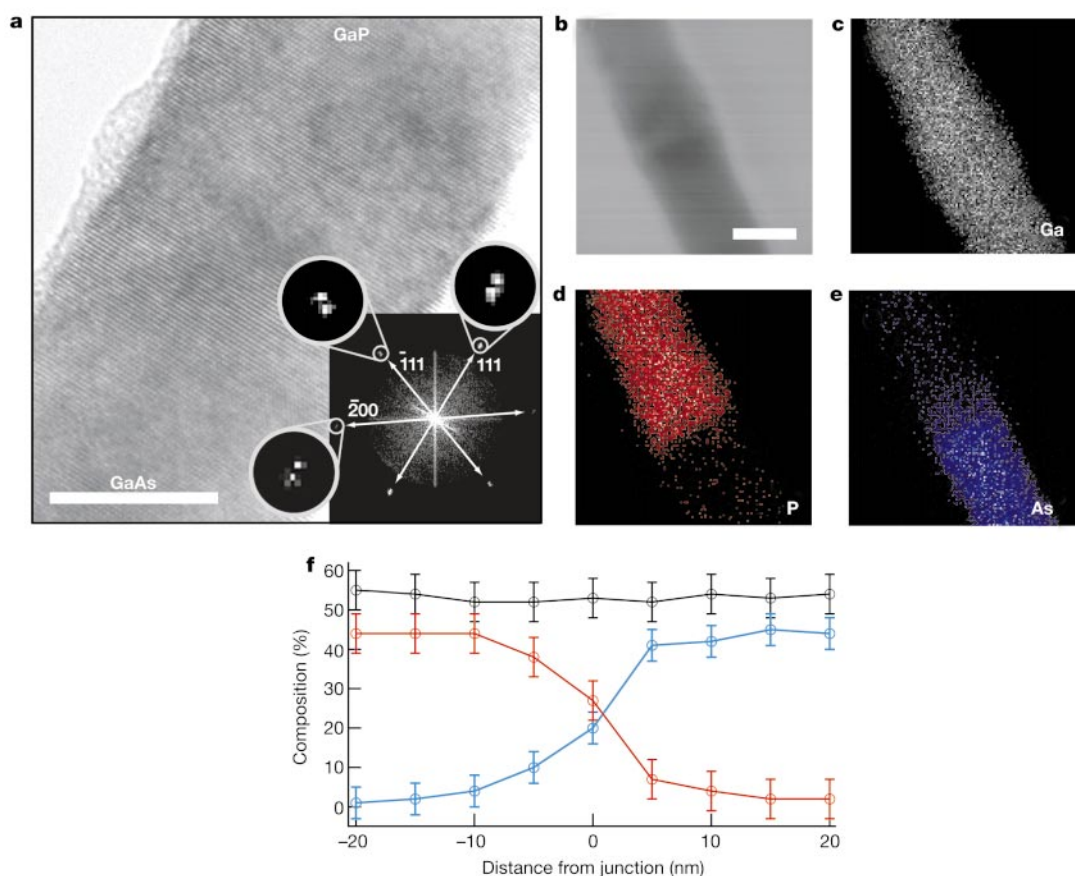


Figure 2 GaAs/GaP nanowire junctions. **a**, High-resolution TEM of a GaAs/GaP junction grown from a 20-nm gold nanocluster catalyst. Scale bar, 10 nm. Inset, two-dimensional Fourier transforms of the entire image show a splitting of the reciprocal lattice peaks along the $\langle 111 \rangle$, $\langle \bar{1}\bar{1}\bar{1} \rangle$ and $\langle 200 \rangle$ lattice directions in the $[0\bar{2}2]$ zone axis, corresponding to the lattice constants for GaAs and GaP (see text). The presence of the heterojunction was confirmed by EDS analysis above and below the junction region (not shown). **b**, TEM image of another junction. Scale bar, 20 nm. **c**, **d**, **e**, Elemental mapping of the Ga (shown

grey), P (red) and As (blue) content of the junction shown in **b**. A scanning TEM was used to take an elemental 'image' of the junction. **f**, Line profiles of the composition through the junction region, showing the change in composition as a function of the distance. The slightly higher Ga (shown black) signal relative to the P (red) and As (blue) signals may be due to uncertainties in the detector calibration or the presence of an amorphous gallium oxide layer around the crystalline nanowire core.

spacer repeats, and ending in a relatively short 4-period (GaAs/GaP) repeat. We consider that in their present form these nanowire superlattice structures could be exploited as optical nanobarcodes¹⁸, which could be useful as labels for imaging. Moreover, the wide range of group III–V and II–VI nanowires that have been

demonstrated previously¹⁶ suggests that it should be possible to encode additional information through variations in the colour of the emitting region using multi-component superlattices. Using materials with a large dielectric contrast might also enable the creation of one-dimensional waveguides¹⁹ with built-in photonic bandgaps, or of cavities for nanowire lasers²⁰.

To assess further the generality of this methodology, we fabricated p–n junctions within individual silicon nanowires by Au-nanocluster-catalysed chemical vapour deposition and dopant modulation^{12,17}. These nanowire p–n junctions were characterized at the single nanowire level by a variety of electrical measurements (Fig. 4) because EDS is insufficiently sensitive to characterize

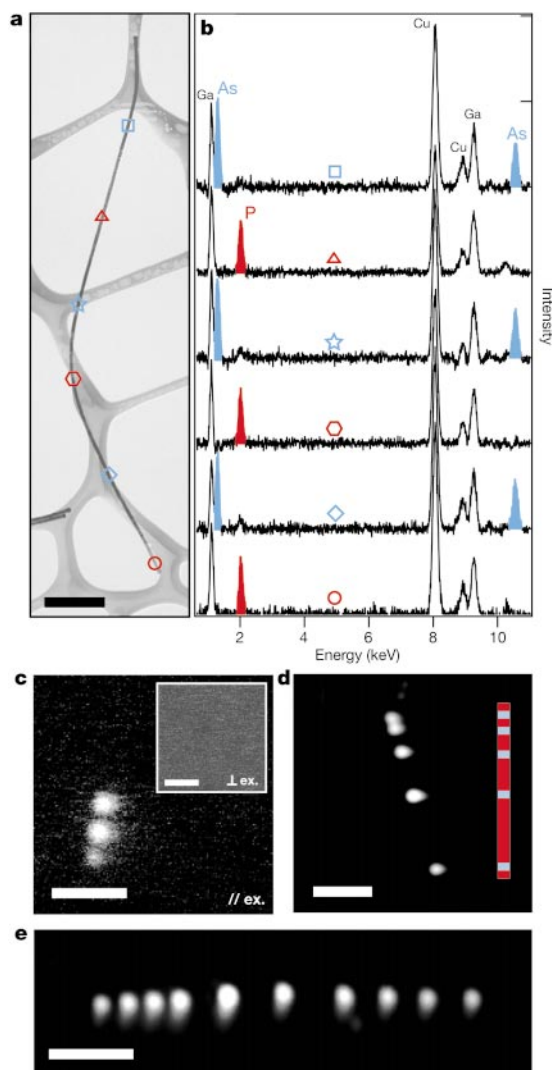


Figure 3 Nanowire superlattice structures. **a**, TEM image of a ~20-nm-diameter (GaP/GaAs)₃ nanowire superlattice. The background mesh is from the holey carbon film, on which the nanowire was deposited for imaging. Scale bar, 300 nm. **b**, Elemental profile of the superlattice along the nanowire length measured by EDS analysis. The symbols in **a** show the location of each EDS spectrum along the nanowire and the colour of the symbol indicates GaP (red) and GaAs (blue) regions. The P K α peak (2.015 keV) is shown in red and the As K α (10.543 keV) and L α (1.282 keV) peaks in blue for clarity. The spectra show clearly a distinct, periodic modulation of the nanowire composition along its entire length, with three uniform periods of GaP, separated by three uniform periods of GaAs. **c**, Photoluminescence image (// excitation) of a nanowire from the same sample as shown in **a** and **b**. The three bright regions correspond to the three GaAs (direct bandgap) regions, while the dark segments are from the GaP (indirect bandgap) regions. Inset, no photoluminescence is observed above background for perpendicular (\perp) excitation due to the dielectric contrast between the nanowire and its surroundings³. Scale bar, 5 μ m. **d**, Photoluminescence image of a 40-nm-diameter GaP(5)/GaAs(5)/GaP(5)/GaAs(5)/GaP(10)/GaAs(5)/GaP(20)/GaAs(5)/GaP(40)/GaAs(5)/GaP(5) superlattice; the numbers in parentheses correspond to the growth times in seconds for each layer. Inset, diagram showing the relative lengths of GaAs (blue) and GaP (red) layers. Scale bar, 5 μ m. **e**, Photoluminescence image of a 21-layer superlattice, (GaP/GaAs)₁₀GaP, showing a group of four equally spaced spots on the left, two in the middle with larger gaps, and another set of four with equal spacing on the end. The superlattice is ~25 μ m in length.

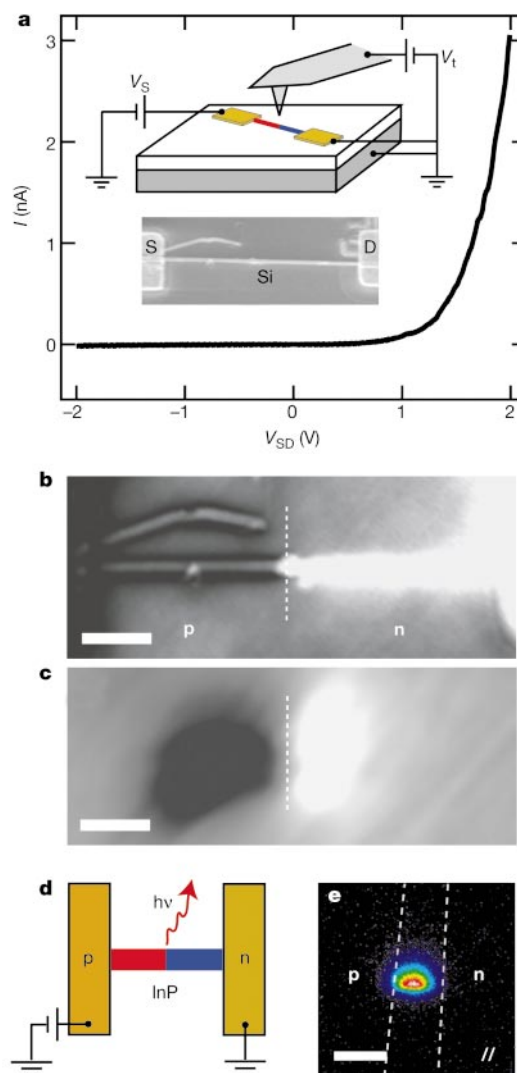


Figure 4 Modulation-doped nanowires. **a**, Inset: a diagram illustrating single-nanowire electrical characterization by transport and probe microscopy, and a scanning electron micrograph of the silicon nanowire device with source (S) and drain (D) electrodes indicated. Main panel, I versus V_{SD} for the silicon nanowire p–n junction. **b**, EFM phase image of the nanowire diode under reverse bias with tip bias (V_t) at +3 V and the drain (right) at +2 V. The signal is proportional to the square of the tip–surface potential difference, and shows an abrupt drop in the middle of the wire at the junction. **c**, SGM image showing the source–drain current as the tip (at +10 V) is scanned across the device. With the drain biased at –2 V ($V_{SD} = +2$ V), bright (dark) regions correspond to an increase (decrease) in the positive quantity I_{SD} . Vertical dashed white lines indicate the junction in **b** and **c**. Scale bars, 500 nm. **d**, Schematic of a InP nanowire LED. **e**, Polarized emission from the LED along the nanowire axis. Dashed white lines indicate the edges of the electrodes in **d**, and were determined from a white light image. No electroluminescence was detected with perpendicular polarization. Scale bar, 3 μ m.

dopant profiles. Current (I) versus voltage (V_{SD}) measurements showed rectifying behaviour consistent with the presence of an intra-nanowire p–n junction (Fig. 4a). To establish that the current rectification was due to intra-nanowire p–n junctions, we characterized the local nanowire potential and gate response by electrostatic force microscopy (EFM) and scanned gate microscopy (SGM), respectively²¹. An EFM image of a typical p–n junction in reverse bias showed that the entire voltage drop occurs at the p–n junction itself (Fig. 4b); EFM measurements showed no potential drop at the contact regions under forward or reverse bias (not shown), ruling out the contact/nanowire interface as the source of rectification in the I – V_{SD} behaviour. In addition, SGM images recorded with the nanowire device in forward bias and the scanned tip–gate positive (Fig. 4c) show enhanced conduction to the right of the junction, indicating an n-type region, and reduced conduction to the left of the junction, indicating depletion of a p-type region. The abrupt change in majority carrier type coincides with the location of the intra-nanowire junction determined by EFM, and thus further confirms that the diode behaviour results from well controlled dopant modulation.

We believe that the direct and controlled growth of nanowire p–n junctions represents an advance over previous work^{8,10,22}. The ability to synthesize modulation-doped nanowire superlattices opens up new opportunities, ranging from ultra-sensitive biological and chemical detectors to bipolar transistors and highly integrated logic gates for nanoelectronics. Moreover, the direct growth of modulation-doped nanowires eliminates the lithographic steps used to create doped nanotube p–n junctions^{8,10}, and thus facilitates the bottom-up assembly of complex functional structures when combined with recent advances in the directed *en masse* organization of nanowire structures^{5,9}.

Last, the use of single InP nanowire p–n junctions as nanoscale LEDs has been investigated (Fig. 4d). I – V_{SD} measurements of InP nanowire p–n structures exhibit rectification similar to that described above for the silicon nanowire p–n junctions. In forward bias, individual InP nanowire devices exhibit light emission from p–n junctions that is both highly polarized and blue-shifted due to the one-dimensional structure and radial quantum confinement, respectively (Fig. 4e)³. The efficiency of these intra-nanowire LEDs is $\sim 0.1\%$, although it can be increased substantially. By defining a quantum dot heterostructure within a p–n diode during nanowire synthesis, it should be possible to engineer an electrically driven single-photon source with well-defined polarization. Such a nanowire device could be extremely useful in quantum cryptography and information processing²³. More generally, we believe that the present results open up many opportunities in nanoscale photonics and electronics, ranging from the relatively simple nanoscale emitters and complementary logic, which can be obtained from single nanowire p–n junctions, to complex periodic superlattices that may enable applications such as nanowire injection lasers and ‘engineered’ one-dimensional electron waveguides. □

Methods

Nanowire synthesis

Nanowires were synthesized either via laser-assisted catalytic growth (GaAs, GaP and InP) or chemical vapour deposition (Si), using Au nanoclusters to direct the growth. Au nanoclusters were deposited onto oxidized silicon substrates and then placed in the reactor furnace. For nanowires produced by laser-assisted catalytic growth, solid targets of GaAs, GaP and InP were ablated using either a pulsed ArF excimer or Nd:YAG lasers, and growth was carried out at 700–850 °C in an argon flow of 100 cm³ STP per minute at 100 torr. A pause of ~ 45 s in the ablation was made between each layer in a given superlattice. Silicon nanowires were grown by chemical vapour deposition at 450 °C using silane (3 cm³ STP per minute) and either 100 p.p.m. diborane (p) or phosphine (n) in helium (18 cm³ STP per minute) as dopants. The furnace was evacuated before switching dopants.

The resulting nanowires were sonicated briefly in ethanol and deposited onto copper grids for TEM analysis. The high-resolution TEM images and EDS spectra from nanowire superlattices were collected on a JEOL 2010F microscope. The elemental mapping of the single junction was conducted on a VG HB603 STEM.

Photoluminescence measurements

Single-nanowire photoluminescence images were obtained using a purpose-built, far-field epifluorescence microscope. Excitation light (488 nm) was focused by an objective (NA = 0.7) to a ~ 30 - μ m-diameter spot at ~ 1.0 kW cm^{−2} on the quartz substrate with dispersed nanowires. A $\lambda/2$ wave plate was used to rotate the polarization of the excitation light, and the resulting photoluminescence was focused and imaged on a liquid-nitrogen-cooled charge coupled device. The emission polarization was measured using a Glan–Thompson polarizer.

Electrical measurements

Nanowires dispersed in ethanol were deposited onto silicon substrates (600-nm oxide), and electrical contacts were defined using electron beam lithography. Ti/Au contacts were used for Si nanowires, and were annealed at 400 °C following deposition. InP LED contacts were fabricated by a two-step process in which the first contact (n-type) was made using Ge/Au or Ni/In/Au and the second (p-type) was made using Zn/Au. The contacts were annealed at 300–350 °C following deposition.

Scanned probe microscopy

A Digital Instruments Nanoscope III with extender module was used for the EFM and SGM measurements. Force modulation etched silicon probe (FESP) tips coated with 5 nm Cr/45 nm Au were used for imaging. For EFM, the nanoscope was operated in lift mode with a lift height of 60 nm and a scan rate of 0.5 Hz.

Received 24 December 2001; accepted 11 January 2002.

- Lieber, C. M. The incredible shrinking circuit. *Sci. Am.* **285**, 58–64 (2001).
- Cui, Y. & Lieber, C. M. Functional nanoscale electronic devices assembled using silicon nanowire building blocks. *Science* **291**, 851–853 (2001).
- Wang, J. F., Gudiksen, M. S., Duan, X. F., Cui, Y. & Lieber, C. M. Highly polarized photoluminescence and photodetection from single indium phosphide nanowires. *Science* **293**, 1455–1457 (2001).
- Cui, Y., Wei, Q. Q., Park, H. K. & Lieber, C. M. Nanowire nanosensors for highly sensitive and selective detection of biological and chemical species. *Science* **293**, 1289–1292 (2001).
- Duan, X. F., Huang, Y., Cui, Y., Wang, J. F. & Lieber, C. M. Indium phosphide nanowires as building blocks for nanoscale electronic and optoelectronic devices. *Nature* **409**, 66–69 (2001).
- Huang, Y. *et al.* Logic gates and computation from assembled nanowire building blocks. *Science* **294**, 1313–1317 (2001).
- Bachtold, A., Hadley, P., Nakanishi, T. & Dekker, C. Logic circuits with carbon nanotube transistors. *Science* **294**, 1317–1320 (2001).
- Derycke, V., Martel, R., Appenzeller, J. & Avouris, P. Carbon nanotube inter- and intramolecular logic gates. *Nano Lett.* **1**, 453–456 (2001).
- Huang, Y., Duan, X. F., Wei, Q. Q. & Lieber, C. M. Directed assembly of one-dimensional nanostructures into functional networks. *Science* **291**, 630–633 (2001).
- Zhou, C. W., Kong, J., Yenilmez, E. & Dai, H. J. Modulated chemical doping of individual carbon nanotubes. *Science* **290**, 1552–1555 (2000).
- Gudiksen, M. S. & Lieber, C. M. Diameter-selective synthesis of semiconductor nanowires. *J. Am. Chem. Soc.* **122**, 8801–8802 (2000).
- Cui, Y., Lauhon, L. J., Gudiksen, M. S., Wang, J. F. & Lieber, C. M. Diameter-controlled synthesis of single-crystal silicon nanowires. *Appl. Phys. Lett.* **78**, 2214–2216 (2001).
- Gudiksen, M. S., Wang, J. F. & Lieber, C. M. Synthetic control of the diameter and length of single crystal semiconductor nanowires. *J. Phys. Chem. B* **105**, 4062–4064 (2001).
- Wagner, R. S. in *Whisker Technology* 47–119 (Wiley-Interscience, New York, 1970).
- Morales, A. M. & Lieber, C. M. A laser ablation method for the synthesis of crystalline semiconductor nanowires. *Science* **279**, 208–211 (1998).
- Duan, X. F. & Lieber, C. M. General synthesis of compound semiconductor nanowires. *Adv. Mater.* **12**, 298–302 (2000).
- Cui, Y., Duan, X. F., Hu, J. T. & Lieber, C. M. Doping and electrical transport in silicon nanowires. *J. Phys. Chem. B* **104**, 5213–5216 (2000).
- Nicewarner-Pena, S. R. *et al.* Submicrometer metallic barcodes. *Science* **294**, 137–141 (2001).
- Chow, E. *et al.* Three-dimensional control of light in a two-dimensional photonic crystal slab. *Nature* **407**, 983–986 (2000).
- Huang, M. H. *et al.* Room-temperature ultraviolet nanowire nanolasers. *Science* **292**, 1897–1899 (2001).
- Bachtold, A. *et al.* Scanned probe microscopy of electronic transport in carbon nanotubes. *Phys. Rev. Lett.* **84**, 6082–6085 (2000).
- Cui, Y., Ouyang, M., Yang, P. & Lieber, C. M. Controlled growth and electrical properties of heterojunctions of carbon nanotubes and silicon nanowires. *Nature* **399**, 48–51 (1999).
- Bennett, C. H. & DiVincenzo, D. P. Quantum information and computation. *Nature* **404**, 247–255 (2000).

Acknowledgements

We thank X. Duan for discussions, and W. MoberlyChan and A. J. Garratt-Reed for assistance with TEM imaging and analysis. M.S.G. thanks the NSF for predoctoral fellowship support. C.M.L. acknowledges support of this work by the Office of Naval Research and Defense Advanced Projects Research Agency.

Competing interests statement

The authors declare that they have no competing financial interests.

Correspondence and requests for materials should be addressed to C.M.L. (e-mail: cml@cmliris.harvard.edu).